GEOPHYSICAL RESEARCH LETTERS, VOL. 24, NO. 7, PAGES 771-774, APRIL 1, 1997

T-matrix computations of zenith-enhanced lidar backscatter from horizontally oriented ice plates

M. I. Mishchenko, D. J. Wielaard, and B. E. Carlson

NASA Goddard Institute for Space Studies, New York, New York

Abstract. Zenith-enhanced backscattering (ZEB) of a lidar beam by cirrus clouds is a remarkable phenomenon usually explained in terms of specular reflection from large plane facets of horizontally oriented ice plates. Since the standard geometric optics approximation (GO) may be inapplicable in many cases, especially in analyzing infrared measurements, and ignores physical optics effects, we use the recently improved exact *T*-matrix method to compute the scattering of light by ice plates at visible and infrared wavelengths. Computations for horizontally and randomly oriented thin disks and oblate spheroids with size parameters up to 50 show that while all particles produce a strong Fraunhofer diffraction peak centered at exactly the forward-scattering direction, a strong and narrow ZEB peak can be produced only by horizontally oriented disks but not by horizontally oriented spheroids or particles in random orientation. This finding demonstrates that ZEB can be produced even by particles which are not in the GO domain of size parameters and supports the traditional interpretation of ZEB. Also, we have found that the angular width of the ZEB peak for horizontally oriented disks is equal to half the width of the Fraunhofer diffraction peak. This result can be used in practice to derive a lower estimate of ice particle sizes from high angular resolution measurements of ZEB. We show that our exact *T*-matrix computations can explain the peculiar zenith-angle dependence of depolarization observed by *Platt et al.* [1978] in the visible and can be interpreted qualitatively in terms of the modified Kirchhoff approximation.

1. Introduction

Many lidar observations of cirrus clouds reveal a strong zenith-enhanced backscatter (ZEB) [*Platt et al.*, 1978; *Thomas et al.*, 1990; *Eberhard*, 1993]. Specifically, the backscattered signal is often found to be extremely strong when the lidar is pointed exactly at zenith and drops dramatically when the direction of the transmitted lidar beam is slightly off zenith. This remarkable phenomenon can only be produced by aligned rather than randomly oriented nonspherical particles and has often been explained in terms of specular reflection of the lidar beam from large plane facets of horizontally oriented ice plates. Theoretical computations of ZEB usually assume that the size of ice particles is much larger than the lidar wavelength, thus making applicable the geometric optics approximation (GO) [*Platt*, 1978]. However, in many cases this may not be true, especially when ZEB is observed in the infrared. Moreover, it is well known that GO computations can be especially inaccurate at exactly the backscattering direction where they fail to reproduce the glory for spherical particles and some depolarization features for nonspherical scatterers [*Hansen and Travis*, 1974; *Mishchenko and Hovenier*, 1995] and considerably overestimate the backscattered intensity for randomly oriented cylindrical particles [*Wielaard et al.*, 1997].

Copyright 1997 by the American Geophysical Union.

Paper number 97GL00545.
0094-8534/97/97GL-00545$05.00

Therefore, in this paper we compute backscattering for horizontally oriented ice plates using the exact *T*-matrix method [*Mishchenko et al.*, 1996a]. Recent significant improvements [*Mishchenko et al.*, 1996a,b; *Wielaard et al.*, 1997] have extended this method to rather large size parameters and have made possible relevant computations for cirrus cloud particles, especially in the infrared. Since this technique is based on directly solving Maxwell's equations, it provides the complete quantitative description of the scattering problem and a verification of the applicability of GO in ZEB computations.

2. Computations and discussion

We specify the direction of the incident beam by zenith angle ϑ and assume that the scattering plane is always the vertical plane containing the incident beam and the normal to the Earth's surface. Assuming that the incident light is linearly polarized and that the scattering ice plates are either randomly oriented in 3D or fully horizontally oriented, we use the standard I_v and I_h Stokes parameters [*Tsang et al.*, 1985] to describe the intensity components polarized in the directions parallel and perpendicular to the vertical scattering plane, respectively, and denote the column composed of I_v and I_h by $\boldsymbol{I}$. The transformation of the Stokes parameters upon single scattering by an ice particle is described by the (ensemble-averaged) Mueller matrix $\boldsymbol{Z}$ as $\boldsymbol{I} = \boldsymbol{Z}\boldsymbol{I}^0/r^2$, where r is the distance between the scattering particle and the observation point. The elements of the Mueller matrix have the dimension of area; the elements Z_{vv} and Z_{hh} are called co-polarized differential scattering cross sections (DSCSs), while Z_{vh} and Z_{hv} are called cross-polarized DSCSs.

We model ice plates as circular disks with a diameter-to-height ratio of 3 and oblate spheroids with an aspect ratio of 3. The disks can represent crystals with large plane facets (e.g., thin hexagonal plates), while spheroids represent ice plates with smooth convex surfaces. We use the *T*-matrix method to compute $\boldsymbol{Z}$ for both randomly and horizontally oriented ice particles at wavelengths $\lambda = 10.75$ and 0.63 μm. The respective refractive indices are $1.0908 + 0.168i$ and $1.3085 + 1.04\times10^{-8}i$ [*Warren*, 1984]. Like all exact techniques for computing nonspherical scattering, the *T*-matrix method has a certain practical limitation on the maximum particle size parameter $x = 2\pi R/\lambda$, where R is the disk radius or the major spheroidal semi-axis. The maximum x for disks was close to 50 at both wavelengths, thus limiting R to approximately 80 μm at $\lambda = 10.75$ μm and $R = 5$ μm at $\lambda = 0.63$ μm. Although the latter radius may be too small to represent cirrus cloud particles in many cases, our results can still be suggestive of the backscattering behavior of real ice plates. Furthermore, recent studies have shown that small ice crystals can be a significant and sometimes even dominant fraction of cirrus cloud particle population (e.g., *Arnott et al.* [1994] and references therein).

We have performed computations for two scattering configurations. In the first configuration the transmitted beam is pointed exactly at zenith and the zenith angle of the scattered light Θ varies from 0 (exact forward scattering) to π (exact backscattering). In the second configuration (the monostatic

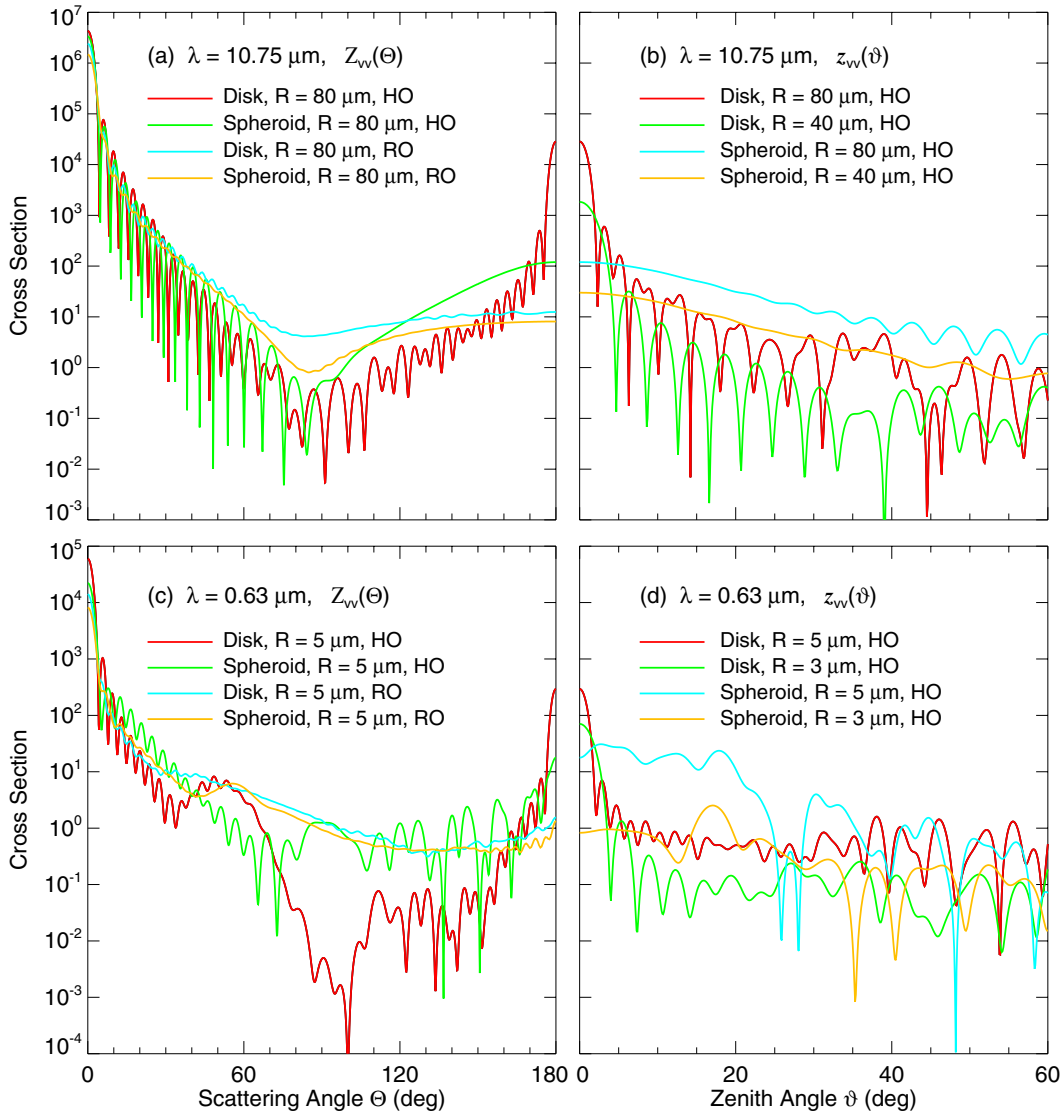

Figure 1. $Z_{vv}(\Theta)$ and $z_{vv}(\vartheta)$ (in μm^2) for monodisperse ice disks and spheroids in horizontal (HO) and random (RO) orientations.

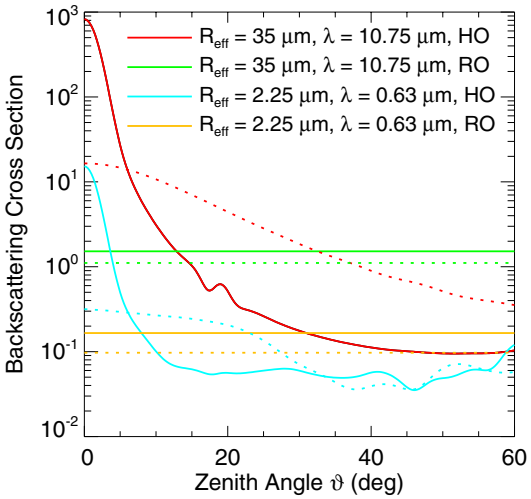

lidar configuration) the direction of scattering is exactly opposite to the direction of illumination and the zenith angle of the lidar beam ϑ varies from 0 (exact zenith) to $\pi/2$ (horizontal pointing). Figure 1 shows the respective co-polarized DSCS $Z_{vv}(\Theta)$ and backscattering cross section $z_{vv}(\vartheta)$ computed for disks and spheroids in horizontal (HO) and random (RO) orientations. Note that for randomly oriented particles $z_{vv}(\vartheta) = \text{const} = Z_{vv}(\pi)$. It is seen from Figures 1(a) and 1(c) that horizontally oriented ice disks produce a strong and narrow backscattering peak as well as a strong Fraunhofer diffraction peak centered at $\Theta = 0$,

Figure 2. $z_{vv}(\vartheta)$ for polydisperse horizontally (HO) and randomly (RO) oriented ice disks (solid curves) and spheroids (dotted curves). The computations assume the standard gamma distribution of disk radii [*Hansen and Travis*, 1974] with the same effective variance $v_{eff} = 0.1$ and effective radii equal to $R_{eff} = 35$ μm at $\lambda = 10.75$ μm and $R_{eff} = 2.25$ μm at $\lambda = 0.63$ μm.

whereas horizontally oriented ice spheroids show only the diffraction peak [cf. *Zuffada and Crisp*, 1997]. The same particles but in random orientation exhibit only the diffraction peak and no strong backscattering enhancement. In addition, Figures 1(b) and 1(d) show that the backscattering enhancement for horizontally oriented disks occurs only when lidar is pointed exactly at zenith and rapidly diminishes as ϑ deviates from 0, thus unequivocally indicating that the peaks in the red and green curves centered at $\vartheta = 0$ represent ZEB. These exact *T*-matrix computations as well as analogous computations at other wavelengths show that horizontally oriented ice disks can produce a strong ZEB even when they have moderate size parameters, whereas convex ice particles with no large plain facets (spheroids) or ice plates in random orientation do not produce anything similar to ZEB.

It should be noted that the pronounced ripple structure seen in the curves for horizontally oriented particles is caused by interference effects [*Mishchenko et al.*, 1996a]. The number and the angular positions of the local maxima and minima vary with particle size. Therefore, size averaging smoothes all oscillations out and makes the resulting polydisperse curves quite smooth (Figure 2). The only exception is the ZEB peak for horizontally oriented disks which is always centered at exactly the backscattering direction and remains intact upon size averaging. Another interesting feature of Figures 1(a) and 1(c) is that the amplitude of the forward-scattering peak for horizontally oriented disks is significantly larger than that for horizontally oriented spheroids with the same R whereas the conventional diffraction theory predicts that the amplitudes should be exactly the same. The difference is especially big (a factor of 2.7) at the nonabsorbing wavelength $\lambda = 0.63$ μm, thus suggesting that it can be explained in GO terms as a manifestation of δ-function transmission through parallel plane facets of the disks [*Takano and Liou*, 1989].

If GO is applied to disks in perfect horizontal orientation, it predicts the angular width of the ZEB peak exactly equal to zero. However, our exact computations for horizontally oriented disks show that the semi-width of the diffraction peak in the $Z_{vv}(\Theta)$ curves (hereafter $\Delta\Theta^D$) is essentially equal to that of the backscattering peak in the same curves (hereafter $\Delta\Theta^B$) and is equal to twice that of the ZEB peak in the $z_{vv}(\vartheta)$ curves (hereafter $\Delta\vartheta^{ZEB}$). It is known that $\Delta\Theta^D$ is completely determined by the particle size parameter x. Therefore, our computations indicate that both $\Delta\Theta^B$ and $\Delta\vartheta^{ZEB}$ for horizontally oriented disks are also fully determined by x.

This remarkable phenomenon can be understood in terms of the so-called modified Kirchhoff approximation [*Jackson*, 1975] applied to large, opaque, horizontally oriented disks with radius much larger than height: $R \gg H$. Indeed, the scattered electric field in the far-field zone ($kr \gg 1$) can be written as the following integral over the particle surface:

$$\boldsymbol{E}_s(\boldsymbol{k}_s) = \frac{e^{ikr}}{4\pi i r}\boldsymbol{k}_s \times \oint dS \left[c\frac{\boldsymbol{k}_s \times \boldsymbol{n} \times \boldsymbol{B}}{k} - \boldsymbol{n} \times \boldsymbol{E} \right] e^{-i\boldsymbol{k}_s \boldsymbol{r}}, \quad (1)$$

where $k = 2\pi/\lambda$, c is the speed of light, $\boldsymbol{k}_s$ is the wave vector in the direction of scattering, $\boldsymbol{n}$ is the local normal to the surface, and $\boldsymbol{E}$ and $\boldsymbol{B}$ are the scattered electric and magnetic fields just outside the particle surface. For a disk with $R \gg H$, the contribution of the side ring surface to the integral (1) is negligibly small. Furthermore, if we assume that the disk is completely opaque, then one of its plane facets will be completely shadowed so that the scattered fields just outside the scatterer will be equal to $-\boldsymbol{E}_0$ and $-\boldsymbol{B}_0$, where $\boldsymbol{E}_0$ and $\boldsymbol{B}_0$ are the incident electric and magnetic fields, respectively, while the other plane facet will be bright with $\boldsymbol{E}$ and $\boldsymbol{B}$ given by the Fresnel equations [*Jackson*, 1975]

$$\boldsymbol{n} \times \boldsymbol{E} = \frac{1-m}{m+1}\boldsymbol{n} \times \boldsymbol{E}_0, \quad \boldsymbol{n} \times \boldsymbol{B} = \frac{m-1}{m+1}\boldsymbol{n} \times \boldsymbol{B}_0, \quad (2)$$

where m is the particle refractive index, and the direction of incidence is assumed to be nearly normal. It is easy to show that the contribution of the shadowed facet to the scattered field is nonzero only in the forward-scattering direction, where it results in the well-known Fraunhofer diffraction peak, and vanishes in the backscattering direction (no backscattering diffraction), whereas the integral over the illuminated facet results in a sharp backscattering peak. Using equations (1) and (2) and the definition of the Mueller matrix, it is rather straightforward to derive the following formulae valid for small Θ and ϑ:

$$Z_{vv}(\Theta) \approx R^4 k^2 \left[\frac{J_1(kR\sin\Theta)}{kR\sin\Theta} \right]^2, \quad (3)$$

$$Z_{vv}(\pi - \Theta) = \frac{|m-1|^2}{|m+1|^2} R^4 k^2 \left[\frac{J_1(kR\sin\Theta)}{kR\sin\Theta} \right]^2, \quad (4)$$

$$z_{vv}(\vartheta) = \cos^2\vartheta \frac{|m-1|^2}{|m+1|^2} R^4 k^2 \left[\frac{J_1(2kR\sin\vartheta)}{2kR\sin\vartheta} \right]^2, \quad (5)$$

where $J_1(y)$ is the Bessel function of the first kind. Equation (3) describes the Fraunhofer diffraction peak, equation (4) describes the backscattering peak in the $Z_{vv}(\Theta)$ curves [cf. *Muinonen*, 1989], and equation (5) describes the ZEB peak. These formulas show that ZEB can indeed be qualitatively interpreted in terms of physical optics and explain why $\Delta\Theta^D \approx \Delta\Theta^B$ and $\Delta\Theta^D \approx 2\,\Delta\vartheta^{ZEB}$ in our *T*-matrix calculations for horizontally oriented disks, why a backscattering lidar peak is observed only in the case of exact vertical illumination ($\vartheta = 0$, equation (5)), and why the diffraction peak for strongly absorbing disks ($\lambda = 10.75$ μm) is about two orders of magnitude stronger than the ZEB peak. (Note that the latter does not hold for nonabsorbing disks due to a strong contribution of internally scattered rays.)

It should be emphasized that equation (3) can be derived for any large particle with a circular projection, thus making the diffraction peak a universal scattering feature, whereas equations (4) and (5) can only be derived under the assumption that the illuminated facet is perfectly flat. This explains why smooth particles like spheroids do not produce a noticeable ZEB peak (Figures 1(b) and 1(d)) and why the $Z_{vv}(\Theta)$ curve for the strongly absorbing horizontally oriented disk (Figure 1(a)) clearly exhibits the contribution described by equation (4), whereas the respective $Z_{vv}(\Theta)$ curve for the horizontally oriented spheroid is featureless at backscattering angles. Similarly, the $z_{vv}(\vartheta)$ curves for absorbing horizontally oriented spheroids (Figure 1(b)) are smooth at small ϑ, whereas the curves for disks show the contribution described by Equation (5).

Since the angular width of the ZEB peak for horizontally oriented disks is completely determined by the particle size parameter, high angular resolution measurements of ZEB can potentially be used to obtain an estimate of the particle size. Unfortunately, in practice one should expect that real ice plates producing ZEB are not perfectly aligned but rather have a small flutter about the horizontal plane. Therefore, the angular profile of the ZEB peak is a convolution of the profile predicted by physical optics and the function describing the distribution of particle orientations. However, since the flutter can only broaden the ZEB peak, measurements of ZEB can still be used to estimate the lower limit of particle sizes.

Our *T*-matrix results also support the explanation by *Platt* [1978] of the peculiar dependence of backscattered intensity and depolarization observed in the visible by *Platt et al.* [1978]. Figure 1 of *Platt et al.* [1978] shows a strong backscattering and

a very low depolarization at $\vartheta = 0°$ and a weak backscattering and a strong depolarization at $\vartheta = 8.2°$. This behavior can be explained by assuming that only a small fraction of ice particles were horizontally oriented plates while the rest of the crystals were randomly oriented. Indeed, assuming incoherent superposition of backscattered radiance, the average backscattering cross section per particle is given by $z_{vv}(\vartheta) = f_H z_{vv}^H(\vartheta) + (1-f_H)z_{vv}^R$, where f_H is the fraction of particles in horizontal orientation, and the backscattering cross section for randomly oriented particles z_{vv}^R is independent of the lidar zenith angle ϑ. At $\vartheta = 0$ the major contribution to $z_{vv}(\vartheta)$ comes from the strong ZEB caused by horizontally oriented plates. At larger zenith angles the ZEB contribution drastically diminishes and $z_{vv}(\vartheta)$ is dominated by a relatively weak backscattering from randomly oriented crystals. Similarly, the linear depolarization ratio for the particle mixture can be written as $\delta(\vartheta) = z_{hv}(\vartheta)/z_{vv}(\vartheta) = (1-f_H)z_{hv}^R/[f_H z_{vv}^H(\vartheta) + (1-f_H)z_{vv}^R]$. In this formula we have taken into account that $z_{hv}^H(\vartheta)$ computed with the *T*-matrix method for horizontally oriented disks is identically equal to zero (thus indicating that the linear depolarization ratio for horizontally oriented disks $z_{hv}^H(\vartheta)/z_{vv}^H(\vartheta)$ is also equal to zero). Our *T*-matrix computations show that for nonabsorbing ice disks and spheroids in random orientation the depolarization ratio z_{hv}^R/z_{vv}^R can exceed 0.6. Therefore, while at $\vartheta = 0°$ the strong ZEB co-polarized contribution makes $\delta(\vartheta)$ small, at larger zenith angles the total depolarization is essentially equal to that of the randomly oriented component and can well reach the values measured by *Platt et al.* [1978].

3. Concluding Remarks

Exact light scattering computations for nonspherical particles are very complicated and, until recently, have not been possible for particles much larger than a wavelength. In this paper we have used the recently improved *T*-matrix method to compute the scattering of light by horizontally and randomly oriented oblate disks and spheroids with size parameters up to 50. Our computations for monodisperse as well as polydisperse particles have shown that ZEB can be produced by ice plates with even modest size parameters. This result is especially important in analyzing observations of cirrus clouds in the infrared, in which case size parameters can be well below 100. We have also found that ZEB can be produced by convex particles only if they have large plane facets (disks), and that the angular width of the ZEB peak depends only on the ratio of the disk radius to the wavelength and is equal to half the width of the Fraunhofer diffraction peak. Both results can be explained in terms of the modified Kirchhoff approximation applied to large thin disks. Furthermore, the second result can be used in practice to estimate the lower limit of ice plate radii. Finally, our exact *T*-matrix computations have shown that horizontally oriented ice plates do not depolarize a vertically pointed lidar beam, whereas the linear depolarization ratio for nonabsorbing ice particles in random orientation can exceed 0.6. These results can explain the peculiar zenith angle dependence of lidar depolarization observed in the visible by *Platt et al.* [1978].

Acknowledgments. We thank two anonymous reviewers for helpful comments and N. T. Zakharova for help with graphics. This work was funded by the NASA FIRE III Project.

References

Arnott, W. P., Y. Y. Dong, J. Hallett, and M. R. Poelott, Role of small ice crystals in radiative properties of cirrus: a case study, FIRE II, November 22, 1991, *J. Geophys. Res.*, *99*, 1371-1381, 1994.

Eberhard, W. L. Cirrus properties deduced from CO_2 lidar observations of zenith-enhanced backscatter from oriented crystals, in *FIRE Cirrus Science Results 1993*, edited by D. S. McDougal, NASA Conf. Publ. 3238, pp. 9-12, 1993.

Jackson, J. D., *Classical Electrodynamics*, John Wiley, New York, 1975.

Hansen, J. E., and L. D. Travis, Light scattering in planetary atmospheres, *Space Sci. Rev.*, *16*, 527-610, 1974.

Mishchenko, M. I., and J. W. Hovenier, Depolarization of light backscattered by randomly oriented nonspherical particles, *Opt. Lett.*, *20*, 1356-1358, 1995.

Mishchenko, M. I., L. D. Travis, and D. W. Mackowski, *T*-matrix computations of light scattering by nonspherical particles: a review, *J. Quant. Spectrosc. Radiat. Transfer*, *55*, 535-575, 1996a.

Mishchenko, M. I., L. D. Travis, and A. Macke, Scattering of light by polydisperse, randomly oriented, finite circular cylinders, *Appl. Opt.*, *55*, 4927-4940, 1996b.

Muinonen, K., Light scattering by randomly oriented crystals, *Appl. Opt.*, *28*, 3051-3060, 1989.

Platt, C. M. R., Lidar backscatter from horizontal ice crystal plates, *J. Appl. Meteorol.*, *17*, 482-488, 1978.

Platt, C. M. R., N. L. Abshire, and G. T. McNice, Some microphysical properties of an ice cloud from lidar observation of horizontally oriented crystals, *J. Appl. Meteorol.*, *17*, 1220-1224, 1978.

Takano, Y., and K.-N. Liou, Solar radiative transfer in cirrus clouds. Part I: Single-scattering and optical properties of hexagonal ice crystals, *J. Atmos. Sci.*, *46*, 3-19, 1989.

Thomas, L., J. C. Cartwright, and D. P. Wareing, Lidar observations of the horizontal orientation of ice crystals in cirrus clouds, *Tellus B*, *42*, 211-216, 1990.

Tsang, L., J. A. Kong, and R. T. Shin, *Theory of Microwave Remote Sensing*, John Wiley, New York, 1985.

Warren, S. G., Optical constants of ice from the ultraviolet to the microwave, *Appl. Opt.*, *23*, 1206-1225, 1984.

Wielaard, D. J., M. I. Mishchenko, A. Macke, and B. E. Carlson, Improved *T*-matrix computations for large, nonabsorbing and weakly absorbing nonspherical particles and comparison with geometric optics approximation, *Appl. Opt.*, in press, 1997.

Zuffada, C., and D. Crisp, Particle scattering in the resonance regime: a full-wave solution for axisymmetric particles with large aspect ratios, *J. Opt. Soc. Am. A*, *14*, 459-469, 1997.

B. E. Carlson, NASA GISS, 2880 Broadway, New York, NY 10025. (e-mail: pabec@giss.nasa.gov)

M. I. Mishchenko, NASA GISS and SUNY/Stony Brook, 2880 Broadway, New York, NY 10025. (e-mail: crmim@giss.nasa. gov)

D. J. Wielaard, NASA GISS and Columbia University, 2880 Broadway, New York, NY 10025. (e-mail: djw@kdist.giss.nasa. gov)

(Received December 12, 1996; revised February 20, 1997; accepted February 24, 1997.)